

A Comparison of Predictive Current Control Schemes for MV Induction Motor Drives

James Scoltock, Tobias Geyer and Udaya Madawala
Department of Electrical and Computer Engineering
The University of Auckland
1052 Auckland, New Zealand

Email: jsc0075@aucklanduni.ac.nz, t.geyer@ieee.org, u.madawala@auckland.ac.nz

Abstract—In medium-voltage drives the switching frequency is limited to a few hundred Hz, necessitating control and modulation schemes capable of producing low levels of current and torque distortions at low switching frequencies. Model Predictive Direct Current Control (MPDCC) has emerged as a promising scheme for medium-voltage induction-motor drives. By forecasting the trajectory of the stator currents over a timespan known as the prediction horizon, MPDCC regulates the stator currents within a set of hysteresis bounds while minimising the inverter switching frequency. Despite the recent surge in popularity of predictive control, such schemes in the field of power electronics and drives were proposed already in the early 1980's. Forced Machine Current Control (FMCC) is an early predictive current control scheme which shares several similarities with MPDCC. However, a comprehensive review and comparison of FMCC with the modern MPDCC scheme has never been carried out. Through simulation, it is shown that the steady state performance of MPDCC and FMCC is similar when the prediction horizon of the former is limited. However, when the prediction horizon is extended, the performance of MPDCC is shown to be superior to FMCC, the horizon of which is inherently restricted.

Index Terms—Model predictive control, current control, medium-voltage drive

I. INTRODUCTION

The inverter-fed induction machine has been a staple of industry for several decades. As expectations regarding motor-drive performance have increased, the traditional control and modulation schemes, which have been applied to machine-side inverters, have been superseded by a number of alternative schemes. Predictive control techniques have recently been applied to motor drives [1] - [5]. The primary attraction of such schemes is their ability to reduce the average switching frequency, and therefore switching losses, of the inverter, while maintaining acceptable levels of harmonic distortion in the current and torque of the machine. In addition to motor drives, predictive control has been applied to active filters, power factor correction and grid-connected converters [6] - [8].

Model Predictive Control (MPC), which was developed in the process control industry in the 1970's [9], has received significant attention from industry. Model Predictive Direct Torque Control (MPDTC), which emerged several years ago, is a variant of MPC and an extension of Direct Torque Control (DTC), which features an online-optimisation process in the control of machine torque [1], [10]. Model Predictive Direct Current Control (MPDCC) is a more recent variant of MPC which treats the machine's stator currents as the variables to be controlled [3], [11].

Although in the field of power electronics and drives MPC has only recently become popular, such schemes were proposed already in the early 1980's. In particular, a Forced

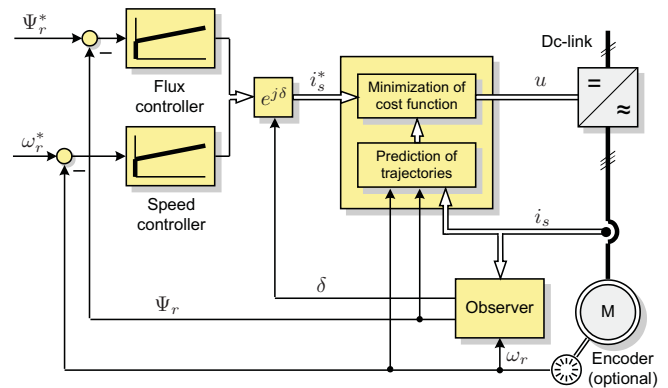


Fig. 1: Predictive current control system setup for a multi-level voltage source inverter driving an electrical machine

Machine Current Control (FMCC) scheme for induction motor drives [12] - [15], first described in 1983 by Holtz and Stadfeld for the control of two-level inverters, shares a number of significant similarities with MPDCC. MPC-based schemes have been extensively compared with carrier-based Pulse Width Modulation (PWM), Space Vector Modulation (SVM) and Optimised Pulse Patterns (OPP) [4]. However, a review and comparison of FMCC against a modern MPC scheme has never been carried out. Such a comparison is useful, as it gives a clear picture of the benefits of modern MPC schemes, relative to early predictive control techniques. The aim of this paper is to therefore describe and benchmark FMCC against the modern MPDCC scheme through simulation of a Medium-Voltage (MV) induction motor drive. The trade off between switching frequency and distortion is a fundamental principle to power converters and will form the basis of comparison. Comparison will be made at steady state, with the key indicators of performance being the inverter switching frequency and the harmonic distortion of the machine's stator currents and torque. The schemes have been compared through a MATLAB-based drive-system simulation which consists of a Neutral Point Clamped (NPC) three-level Voltage Source Inverter (VSI) driving a squirrel-cage Induction Motor (IM). Since the aim of this comparison is to gauge the quality of the control schemes in as general a sense as possible, effects such as deadtime, measurement noise and controller delay have been neglected.

II. DRIVE SYSTEM

A. System Setup

As shown in Fig. 1, the drive system used in this paper utilises an inner and outer control loop. The outer speed and

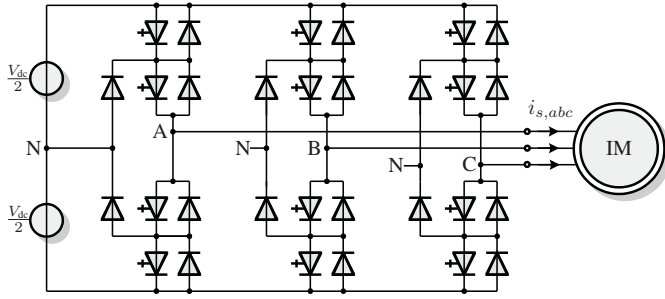


Fig. 2: Three-level neutral point clamped voltage source inverter driving an induction motor with a fixed neutral point potential

flux regulators are PI controllers which regulate the stator current reference value based on the speed and rotor flux references. The outer loop operates in the rotating dq reference frame. The inner predictive loop makes switching decisions based on state feedback and the current reference provided by the outer controllers. It is the inner loop which relates to the predictive control schemes described in this paper.

B. Inverter Model

The typical setup for a three-level NPC inverter driving an IM is shown in Fig 2. Each phase leg is able to assume one of three states, which may be represented by the integer variables $u_a, u_b, u_c \in \{-1, 0, 1\}$. With three voltage levels per phase and three phases, there are $3^3 = 27$ possible switching states of the form $u_{abc} = [u_a u_b u_c]^T$. Within those states, 19 distinct voltage vectors exist which the inverter is capable of producing. The voltage vectors can be represented by transforming the switching states from the three-phase abc system to the orthogonal $\alpha\beta$ system. The corresponding voltage at the machine terminals is given by

$$v_{\alpha\beta} = \frac{V_{dc}}{2} P u_{abc} \quad (1)$$

where $v_{\alpha\beta} = [v_\alpha v_\beta]^T$, V_{dc} is the DC-link voltage and P is the transformation matrix

$$P = \frac{2}{3} \begin{bmatrix} 1 & -\frac{1}{2} & -\frac{1}{2} \\ 0 & \frac{\sqrt{3}}{2} & -\frac{\sqrt{3}}{2} \end{bmatrix}. \quad (2)$$

In the inverter under consideration all switching transitions are allowed except for those which involve switching between the upper and lower rails. For example, a transition from $u_{abc} = [1 1 1]^T$ to $[0 0 1]^T$ is allowed, whereas a transition to $[-1 1 1]^T$ is not.

C. Induction Machine Model

The IM is modeled in the $\alpha\beta$ reference frame, with the mechanical load assumed to be constant. The system state variables are the $\alpha\beta$ components of the stator currents and rotor fluxes, $i_{s\alpha}$, $i_{s\beta}$, $\Psi_{r\alpha}$ and $\Psi_{r\beta}$ respectively. The input vector is the three-phase switch position u_{abc} . The model parameters are the angular velocity of the rotor, ω_r , the resistances of the stator and rotor r_s and r_r respectively, the reactances of the stator and rotor x_{ls} and x_{lr} respectively, the mutual reactance x_m , the mechanical inertia of the load, J , and the mechanical torque of the load, T_l . With $x = [i_{s\alpha} i_{s\beta} \Psi_{r\alpha} \Psi_{r\beta}]^T$ and

$u = [u_a u_b u_c]^T$ we can define the continuous-time state equation of the system as [16]

$$\frac{dx}{dt} = Ax + Bu \quad (3)$$

with A being the state matrix

$$A = \begin{bmatrix} -\frac{1}{\tau_\sigma'} & 0 & \frac{k_r}{r_\sigma \tau_r \tau_\sigma'} & \frac{k_r \omega_r}{r_\sigma \tau_r \tau_\sigma'} \\ 0 & -\frac{1}{\tau_\sigma'} & -\frac{k_r \omega_r}{r_\sigma \tau_r \tau_\sigma'} & \frac{k_r}{r_\sigma \tau_r \tau_\sigma'} \\ \frac{x_m}{\tau_r} & 0 & -\frac{1}{\tau_r} & -\omega_r \\ 0 & \frac{x_m}{\tau_r} & \omega_r & -\frac{1}{\tau_r} \end{bmatrix} \quad (4)$$

and B the input matrix

$$B = \begin{bmatrix} \frac{1}{r_\sigma \tau_\sigma'} & 0 & 0 & 0 \\ 0 & \frac{1}{r_\sigma \tau_\sigma'} & 0 & 0 \end{bmatrix}^T \frac{V_{dc}}{2} P \quad (5)$$

with the electromagnetic torque, T_e , given by

$$T_e = k_r (i_{s\beta} \Psi_{r\alpha} - i_{s\alpha} \Psi_{r\beta}) \quad (6)$$

and the relationship between rotor speed and torque

$$\frac{d\omega_r}{dt} = \frac{1}{J} (T_e - T_l). \quad (7)$$

The deduced parameters used in the above equations are the rotor coupling factor $k_r = \frac{x_m}{x_r}$, total leakage factor $\sigma = 1 - \frac{x_m^2}{x_s x_r}$, leakage reactance $x_\sigma = \sigma x_s$, where $x_s = x_{ls} + x_m$ and $x_r = x_{lr} + x_m$, and equivalent resistance $r_\sigma = r_s + k_r^2 r_r$. The deduced time constants include the transient stator time constant $\tau_\sigma' = \frac{\sigma x_s}{r_\sigma}$, and the rotor time constant $\tau_r = \frac{x_r}{r_r}$.

Equations (3) – (7) provide a complete description of the dynamic behaviour of the IM when non-idealities such as magnetic saturation, the skin effect and variations in the rotor resistance are ignored.

D. Internal Model of the Controller

In order for a predictive control scheme to be implemented, a discrete-time model of the drive is required to serve as an internal prediction model for the controller. The model's purpose is to predict the trajectory of the stator currents and rotor fluxes over as many sampling intervals as are required. Due to the fact that the rotor time constant greatly exceeds the length of a prediction horizon, the rotor speed is assumed to be constant within the prediction horizon and is treated as a model parameter rather than an additional variable [3], [11]. From the continuous time state equation of (3) – (5), and with the output vector defined as $y = [i_{s\alpha} i_{s\beta}]^T$, the following discrete-time model of the drive can be derived

$$x(k+1) = (I + T_s A)x(k) + T_s B u(k) \quad (8a)$$

$$y(k) = C x(k) \quad (8b)$$

where I is the 4x4 identity matrix, T_s is the sampling time of 25 μs and C is the output matrix

$$C = \begin{bmatrix} 1 & 0 & 0 & 0 \\ 0 & 1 & 0 & 0 \end{bmatrix}. \quad (9)$$

III. CONTROL SCHEMES

Both MPDCC and FMCC replace the inner current control loop and modulator of traditional Field Oriented Control (FOC) schemes with a single online-optimisation stage. In doing so, MPDCC and FMCC are able to address the control and modulation problems simultaneously by directly manipulating the switching state of the inverter. A boundary area is defined around the stator current reference i_s^* , with the objective of the controller being to keep the stator current i_s inside the boundary area while minimising the switching frequency or switching losses of the inverter. The dimension of the boundary area determines the current ripple, and therefore Total Demand Distortion (TDD), of the stator current, and in doing so sets the trade-off between switching frequency (or losses) and current distortion.

A. Model Predictive Direct Current Control (MPDCC)

In MPDCC, symmetrical hysteresis bounds are defined around each of the abc stator currents. δ_i denotes the difference between the upper (or lower) bound and the reference. The aim of the controller is subsequently to keep each of the stator currents within the bounds while minimising the switching frequency of the inverter.

It is important to clearly differentiate the switching horizon N_s from the prediction horizon N_p . The switching horizon refers to the number of switching events within the horizon, while the prediction horizon refers to the number of time-steps the controller looks forward, starting from the current time-step k . The switching horizon is composed of the elements 'S' and 'E', which stand for switch and extend, respectively. During the extension steps, which occur between and after the switching events (with the switching state held constant), the trajectory of the outputs is extended until one or more bounds are violated. Extension may either be exact, utilising the internal model of the controller, or an approximation based on linear or quadratic extrapolation or interpolation [17]. By utilising extension steps, a short switching horizon including only one to three 'S' events may result in a prediction horizon of 30 to more than 100 steps.

By lengthening the switching horizon, the controller is able to look further into the future and make better informed switching decisions. One could therefore expect an improvement in performance, for example a reduced switching frequency for the same current distortion, by extending the switching horizon from 'eSE' to 'eSESESE'. Note that the lower case 'e' refers to an optional extension event at the beginning of the horizon.

At each time-step k the set of allowable switching sequences forward in time is determined for the switching horizon N_s based on the current switching state $u(k-1)$. For each sequence, the trajectory of the output currents forward in time is predicted using the internal model of the controller. For each sequence, the output trajectory must remain a candidate over the entire prediction horizon N_p . A candidate sequence is one for which all of the output variables are either feasible, or pointing in the correct direction. An output variable is feasible if it lies within its hysteresis bounds. Pointing in the correct direction denotes the instance where an output variable lies outside the bounds, but moves closer to it at every time-step of the prediction horizon. For a given switching horizon, each candidate sequence $U^i(k) = [u^i(k), u^i(k+1), \dots, u^i(k+N_p^i-1)]$

yields an associated cost which can be determined from

$$C^i = \frac{1}{N_p^i} \sum_{\ell=k}^{k+N_p^i-1} \|u^i(\ell) - u^i(\ell-1)\|_1 \quad (10)$$

for minimisation of switching frequency, or

$$C^i = \frac{E^i}{N_p^i} \quad (11)$$

for minimisation of switching losses, where E^i is the total switching energy loss over the prediction horizon. A detailed description of the calculation of switching losses is given in [10]. The switching sequence $U^i(k)$ with the minimal cost is subsequently determined

$$i = \arg \min C^i \quad (12)$$

with the switching state $u(k) = u^i(k)$ applied. The horizon is subsequently shifted one step forward, with the process repeated at $k+1$. [3] and [10] provide further details on the MPDCC problem and control procedure.

In order to simplify the problem, MPDCC can be reformulated in the $\alpha\beta$ -plane. By transforming the abc hysteresis bounds to the $\alpha\beta$ -plane, a hexagonal boundary area centred on the reference current $i_{s,\alpha\beta}^*$ results. The problem can be further transformed to the dq -reference plane, which results in a hexagonal-boundary area centred on the stationary reference current $i_{s,dq}^*$. Due to the synchronously-rotating nature of the dq -plane, the hexagonal boundary is not fixed in space. As shown in Fig. 3a, the boundary area rotates at the angular speed of the rotor flux, ω_s , in an anti-clockwise direction.

Fig. 3a also illustrates an example output prediction for an arbitrary switching sequence over a switching horizon of 'SESESE'. At time-step k switching is necessitated due to imminent violation of the boundary area. Following extension, switching subsequently occurs at time-steps $k+N_{p1}$ and $k+N_{p2}$. The final extension leg of the horizon results in a total prediction horizon of length N_p time-steps. Note that in Fig. 3a all trajectories are referred to the position of the boundary area at time-step k .

B. Forced Machine Current Control (FMCC)

Unlike MPDCC, where the bounds are defined around each of the phase currents separately, FMCC as described in [12], utilises instead a radial boundary area defined around the stator current reference on the $\alpha\beta$ -plane. δ_r denotes the radius of the boundary area. Like MPDCC, FMCC aims to keep the output current regulated about the reference while minimising the switching frequency of the inverter. The problem can be simplified by transforming it to the dq -plane, which results in a fixed reference current $i_{s,dq}^*$ and boundary area as shown in Fig. 3b.

Unlike MPDCC, where the switching horizon is variable and can be made up of a variety of 'S' and 'E' elements, the switching horizon for FMCC is effectively limited to 'SE', thus restricting the length of the prediction horizon. The control procedure for FMCC is similar to that of MPDCC. At each time-step k the stator current of the machine is sampled, and any intersection of the current trajectory with the boundary circle detected. When an intersection is detected (meaning the stator current vector lies outside the boundary area) the set of allowable switching states which can be applied to the inverter

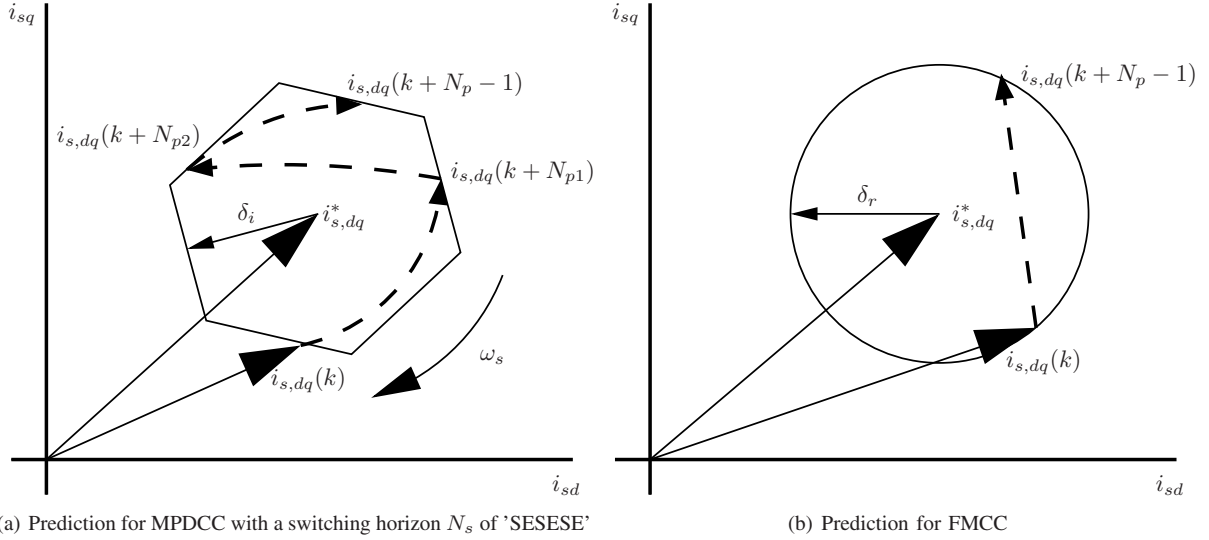


Fig. 3: Comparison of the boundary areas and prediction sequences for MPDCC and FMCC on the dq -plane.

at time-step k is determined based on the current switching state $u(k-1)$. For each allowable switching state which can be applied at time-step k , the trajectory of the output currents is predicted forward in time using a linear approximation technique as described in [12] - [14]. During extension, the switching state is held constant until another intersection of the boundary area occurs. Each candidate switching state $u^i(k)$ will yield a prediction horizon of length N_p^i , where N_p is the number of time-steps from the switching time-step k to the next intersection of the boundary. Since FMCC minimises the switching frequency of the inverter, the cost associated with each switching state can be determined from (10) with the optimal state being that which minimises (12). Fig. 3b illustrates an example output prediction for an arbitrary switching state. At time-step k switching is necessitated due to the output current intersecting the boundary circle. The trajectory of the output current is predicted for the candidate switching state $u(k)$, with extension of the current trajectory resulting in a prediction horizon of length N_p .

In addition to the FMCC scheme outlined above, several variant FMCC schemes were proposed. In [14], Holtz and Stadtfeld proposed a method of optimisation by double prediction, where the controller preemptively selects a new switching state in order to avoid intersection of the boundary. This has the benefit of enforcing strict observance of the stator current boundary, as is the case for MPDCC with a horizon of the form 'eSE'. In [13] and [15], a variant of FMCC which utilises a rectangular boundary area around the stator current reference was proposed. This allows the torque and current distortion to be controlled with a large degree of independence, through variation of the height and width of the rectangle. The use of a rectangular boundary area parallels MPDCC, where the boundary area is defined such that the machine torque is directly controlled.

IV. PERFORMANCE EVALUATION

This section summarizes the performance of MPDCC and FMCC for simulations carried out using the drive system outlined in Section II. A 3.3 kV, 50 Hz, 2 MVA squirrel-cage IM has been used, a typical machine used in the MV drive

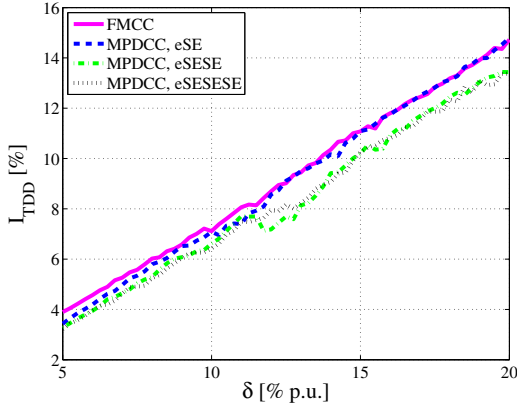
industry. The NPC inverter has a total nominal DC-link voltage of 5.2 kV. ABB's 35L4510 4.5 kV 4 kA Integrated Gate Commutated Thyristor (IGCT) is used for all switches. ABBs 10H4520 fast recovery diode is used for all diodes. A summary of the machine and inverter parameters can be found in Table I. The p.u. system uses base values of $V_B = \sqrt{2/3}V_{rat} = 2694$ V, $I_B = \sqrt{2}I_{rat} = 504$ A, and $f_B = f_{rat} = 50$ Hz.

In order to gauge the performance of MPDCC and FMCC, three well known modulation schemes – carrier-based PWM, SVM and OPP – have been included for comparison, which have been used for benchmarking in previous papers on MPC in [3] and [4]. The carrier-based PWM and SVM modulation schemes have been studied extensively and are common in industry, and as such provide useful performance references for the predictive control schemes. OPPs, which are calculated off-line, minimize the current distortion for a given pulse number (switching frequency). This is done through optimisation of the switching angles for all possible operating points over a quarter of a fundamental period. The steady state performance of OPP provides a useful benchmark for predictive schemes, which aim to achieve optimal results through online optimisation.

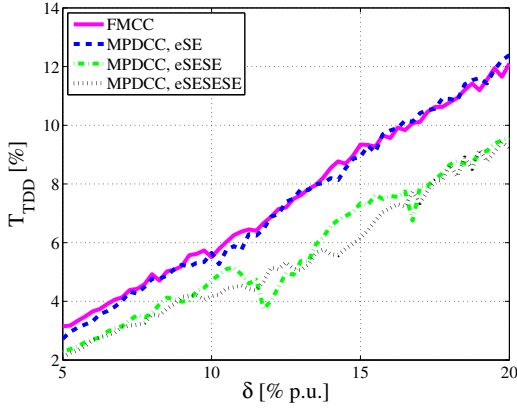
Simulations were run at 60% speed and full torque at steady state. All simulations have been carried out under the assumption of a fixed neutral point. MPDCC simulations have been run with switching horizons of 'eSE', 'eSESE', and 'eSESESE', and with the cost function penalising the inverter switching frequency. For FMCC, all simulations have been run with a circular boundary area and single prediction. In addition, all extension steps for both MPDCC and FMCC

TABLE I: Rated values (left) and parameters (right) of the drive model used

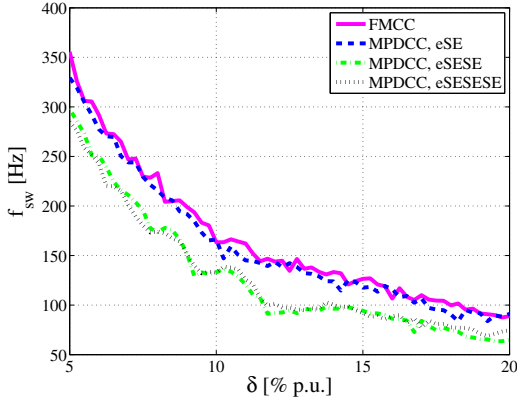
Induction Motor			
Voltage	3300 V	r_s	0.0108 pu
Current	356 A	r_r	0.0091 pu
Real power	1.587 MW	x_{ls}	0.1493 pu
Apparent power	2.035 MVA	x_{lr}	0.1104 pu
Frequency	50 Hz	x_m	2.3489 pu
Rotational speed	596 rpm		
Inverter			
DC-link voltage	5200 V	V_{dc}	1.930 pu



(a) Current TDD vs bound width.



(b) Torque TDD vs bound width.



(c) Switching frequency vs bound width.

Fig. 4: Performance trade-off for MPDCC with switching horizons of 'eSE', 'eSESE' and 'eSESESE' and FMCC. Each plot shows the variation of a different performance metric as the boundary dimensions (δ_i for MPDCC, δ_r for FMCC) are varied from 5% to 20% p.u. at increments of 0.25%. The operating point is $\omega_e = 0.6$ p.u., $T_e = 1$ p.u. At all points, each scheme was simulated over 20 fundamental periods.

utilise the internal control model, rather than a linear or quadratic extrapolation technique. Although FMCC was originally proposed with linear extrapolation, as this was the only feasible technique at the time, the use of the internal control model allows a fairer comparison with MPDCC. Simulations have been run with the outer flux and speed controllers turned off, with the fixed current reference corresponding to torque and flux references of 1 p.u.

Fig. 4 shows that MPDCC with a short horizon of 'eSE' and FMCC achieve similar levels of current TDD, torque TDD, and switching frequency as the bound width is varied. This is to be expected, as the boundary areas for MPDCC and FMCC are similarly defined, and when MPDCC is limited to a switching horizon of 'eSE', the control procedures are very similar. For medium and long horizons of 'eSESE' and 'eSESESE', MPDCC performs significantly better than FMCC, yielding considerably lower current and torque TDD and switching frequency across all bound widths. It is interesting to note that little improvement is exhibited when extending the horizon from 'eSESE' to 'eSESESE'. This could be due to the fact that the cost function here is penalising switching frequency rather than switching losses.

It is interesting to note the lower current and torque TDD yielded by MPDCC relative to FMCC. This is likely a result of the boundary shapes of MPDCC and FMCC. The hexagonal boundary area of MPDCC results in a constant and symmetrical ripple for each phase current, whereas the circular boundary of FMCC results in a non-constant ripple for each phase current and a higher level of distortion. Table II summarises the relative performance of MPDCC for short, medium and long switching horizons against FMCC. The similarity between MPDCC with a short horizon and FMCC is obvious, with MPDCC with a horizon of 'eSE' on average improving on FMCC by only a few percent for switching frequency and current TDD, and showing no improvement in terms of torque TDD. The reduction in current and torque TDD for MPDCC with medium and long switching horizons is far more notable, however. The long horizon of 'eSESESE' yields a torque TDD 27% lower than FMCC and a current TDD almost 10% lower than FMCC on average. Additionally, for both medium and long horizons the switching frequency relative to FMCC is reduced by around 20% on average.

Table III compares FMCC and MPDCC with carrier-based PWM, SVM and OPP at two points – one at a current TDD of approximately 4%, the other at a switching frequency of approximately 180 Hz. At a current TDD of about 4%, MPDCC with a short horizon yields a switching frequency 10.5% lower and switching losses 2% lower than FMCC. For a long horizon of 'eSESESE', MPDCC results in a switching frequency 25.5% lower and switching losses 23.5% lower than FMCC. However, FMCC improves on the switching frequency and switching losses of PWM by 19.5% and 9.9%, respectively. When compared to OPP, all of the predictive schemes fall short in terms of switching frequency and losses, however with medium and long horizons MPDCC achieves a marginally lower torque TDD than OPP. It is interesting to note that both PWM and SVM yield substantially lower torque TDD than both FMCC and MPDCC.

TABLE II: Comparison of FMCC with MPDCC. The table shows the average percentage values of current distortion I_{TDD} , torque distortion T_{TDD} and switching frequency f_{sw} relative to FMCC. Each value represents the average from across the range of bound widths.

Control scheme	Switching horizon	f_{sw} [%]	I_{TDD} [%]	T_{TDD} [%]
FMCC	-	100	100	100
MPDCC	eSE	96.2	97.8	100
MPDCC	eSESE	77.6	91.3	77.0
MPDCC	eSESESE	77.8	90.2	73.0

TABLE III: Comparison of FMCC with MPDCC, carrier-based PWM, SVM and OPP. The first comparison is at a current TDD of approximately 4%, while the second is at a switching frequency of about 180 Hz. The first section summarises the control settings, the second the absolute values summarising performance, and the third section the performance values relative to carrier-based PWM. f_c denotes the carrier frequency of PWM/SVM, while d denotes the pulse number for OPP.

Control scheme	Control setting	Switching horizon	f_{sw} [Hz]	I_{TDD} [%]	T_{TDD} [%]	P_{sw} [kW]	f_{sw} [%]	I_{TDD} [%]	T_{TDD} [%]	P_{sw} [%]
PWM	$f_c = 780$ Hz	-	400	3.97	1.34	9.40	100	100	100	100
SVM	$f_c = 570$ Hz	-	300	3.92	1.59	6.88	74.1	98.7	119	73.2
FMCC	$\delta_r = 0.0525$	-	326	4.05	3.17	8.47	80.5	102	237	90.1
MPDCC	$\delta_i = 0.0575$	eSE	292	4.02	3.21	8.30	72.1	101	240	88.9
MPDCC	$\delta_i = 0.0600$	eSESE	250	3.94	2.70	6.82	61.7	99.2	201	72.6
MPDCC	$\delta_i = 0.0600$	eSESESE	243	3.98	2.67	6.48	60.0	100	199	68.9
OPP	$d = 7$	-	210	4.04	2.71	5.24	52.8	102	202	55.7
PWM	$f_c = 330$ Hz	-	180	9.45	3.20	4.31	100	100	100	100
SVM	$f_c = 330$ Hz	-	180	6.88	2.89	4.27	100	72.8	90.3	99.1
FMCC	$\delta_r = 0.0975$	-	180	7.22	5.73	4.85	100	76.4	179	113
MPDCC	$\delta_i = 0.0925$	eSE	185	6.54	5.18	5.03	103	69.2	162	117
MPDCC	$\delta_i = 0.0825$	eSESE	178	5.58	3.89	4.69	98.9	59.0	122	109
MPDCC	$\delta_i = 0.0750$	eSESESE	180	4.91	3.20	4.86	100	52.0	100	113
OPP	$d = 6$	-	180	4.46	2.55	4.45	102	47.2	79.7	103

At a switching frequency of about 180 Hz, MPDCC with a short horizon yields a current TDD 10.4% lower and torque TDD 10.6% lower than FMCC. With a long horizon, these reductions are 32% and 44%, respectively. However, FMCC improves on the current TDD of PWM by 23.6% and achieves a similar level of current TDD to SVM. When compared to OPP, the predictive schemes all produce higher levels of current and torque TDD.

V. CONCLUSION

This paper has presented a review of FMCC and a comparison against the more recent MPDCC. Initially proposed for two-level inverters, FMCC has here been extended to a three-level topology with a model-based prediction technique utilised, in order to allow comparison with MPDCC. An internal control model for the drive system has been derived, and the conceptual similarity between FMCC and MPDCC summarised. FMCC has been shown to perform to a similar level as MPDCC when the horizon is short. However, as the switching horizon is lengthened, MPDCC performs to a higher level than FMCC. Despite this, it is important to note that at the time when FMCC was conceived in the early 1980s, the computational power required for long switching horizons was unavailable, and it remains a very good control scheme when computational resources are restricted. In addition, the performance of FMCC could be improved with the addition of double prediction. Both FMCC and MDPCC have been shown to perform to a higher level than carrier-based PWM in terms of current TDD and switching frequency. The torque TDD is in general poorer for the predictive control schemes than for both carrier-based PWM and SVM. If minimisation of torque TDD is a priority, then MPDTC or FMCC with a rectangular boundary area are better options, as the hysteresis bounds for such schemes are shaped to minimise the torque ripple.

REFERENCES

- [1] T. Geyer, G. Papafioti, and M. Morari. Model predictive direct torque control - part I: Concept, algorithm and analysis. *IEEE Trans. Ind. Electron.*, 56(6):1894–1905, Jun. 2009.
- [2] G. Papafioti, J. Kley, K.G. Papadopoulos, P. Bohren, and M. Morari. Model predictive direct torque control - part II: Implementation and experimental evaluation. *IEEE Trans. Ind. Electron.*, 56(6):1906–1915, Jun. 2009.
- [3] T. Geyer. Model predictive direct current control for multi-level converters. In *Proc. IEEE Energy Conv. Congr. and Exp.*, Atlanta, USA, Sep. 2010.
- [4] T. Geyer. A comparison of control and modulation schemes for medium-voltage drives: emerging predictive control concepts versus field oriented control. In *Proc. IEEE Energy Conv. Congr. and Exp.*, Atlanta, USA, Sep. 2010.
- [5] P. Cortés, M. P. Kazmierkowski, R. M. Kennel, D. E. Quevedo, and J. Rodríguez. Predictive control in power electronics and drives. *IEEE Trans. Ind. Electron.*, 55(12):4312–4324, Dec. 2008.
- [6] R. Vargas, P. Cortés, U. Ammann, J. Rodríguez, and J. Pontt. Predictive control of a three-phase neutral-point-clamped inverter. *IEEE Trans. Ind. Electron.*, 54(5):2697–2705, Oct. 2007.
- [7] J.M. Espi Huerta, J. Castello-Moreno, J.R. Fischer, and R. Garcia-Gil. A synchronous reference frame robust predictive current control for three-phase grid-connected inverters. *IEEE Trans. Ind. Electron.*, 57(3):954–962, Mar. 2010.
- [8] P. Cortés, G. Ortiz, J.I. Yuz, J. Rodriguez, S. Vazquez, and L.G. Franquelo. Model predictive control of an inverter with output LC filter for UPS applications. *IEEE Trans. Ind. Electron.*, 56(6):1875–1883, Jun. 2009.
- [9] D. Q. Mayne, J. B. Rawlings, C. V. Rao, and P. O. M. Scaokaert. Constrained model predictive control: Stability and optimality. *Automatica*, 36(6):789–814, Jun. 2000.
- [10] T. Geyer. Generalized model predictive direct torque control: Long prediction horizons and minimization of switching losses. In *Proc. IEEE Conf. on Decis. and Control*, Shanghai, China, Dec. 2009.
- [11] J. C. Ramirez Martinez, R. M. Kennel, and T. Geyer. Model predictive direct current control. In *Proc. IEEE Int. Conf. on Ind. Techn.*, Vina del Mar, Chile, Mar. 2010.
- [12] J. Holtz and S. Stadtfeld. A predictive controller for the stator current vector of ac machines fed from a switched voltage source. In *Proc. Int. Power Electron. Conf.*, Tokyo, Japan, 1983.
- [13] J. Holtz and S. Stadtfeld. Field-oriented control by forced motor currents in a voltage fed inverter drive. In *Proc. 3rd IFAC Symp. on Control in Power Electron. and Elect. Drives*, Lausanne, Switzerland, Sep. 1983.
- [14] J. Holtz and S. Stadtfeld. A PWM inverter drive system with on-line optimized pulse patterns. In *Proc. 1st Eur. Conf. on Power Electron. and Appl.*, Brussels, Belgium, Oct. 1985.
- [15] A. Khambadkone and J. Holtz. Low switching frequency and high dynamic pulsewidth modulation based on field-orientation for high-power inverter drive. *IEEE Trans. Power Electron.*, 7(4):627–632, Oct. 1992.
- [16] P. C. Krause, O. Wasynczuk, and S. D. Sudhoff. *Analysis of Electric Machinery and Drive Systems*. Intersci. Publ. John Wiley & Sons Inc., 2002.
- [17] Y. Zeinaly, T. Geyer, and B. Egardt. Trajectory extension methods for model predictive direct torque control. In *Proc. IEEE App. Power Electron. Conf. and Exp.*, Fort Worth, USA, Mar. 2011.